in Figs. 2 (e) and (f), when $T_1 / T_g \leq 0.85$, $C_R > 1$; when $0.85 < T_1 / T_g \leq 1.2$, $C_R < 1$; and when $T_1 / T_g > 1.2$, $C_R \approx 1$. It is observed that the equal displacement assumption is likely to underestimate the inelastic displacement demand of SC systems.

4.2 Effect of model parameters on the constant-strength inelastic displacement ratio C_R

4.2.1 Influence of response reduction factor R

The constant-strength inelastic displacement ratio C_R increases with an increase in R (see Fig. 3). However, it tends to remain constant when $R \geq 10$ for $T_1 / T_g < 0.85$. The effect of R is not significant for $0.85 < T_1 / T_g \leq 1.2$ (Figs. 2 (e) and (f)), however a small increase in C_R as R increases were observed for $T_1 / T_g > 1.2$. This trend of variation of C_R with R is similar, regardless of β value.

4.2.2 Influence of hysteretic energy dissipation parameter β

The added energy dissipation in addition to assumed 5% inherent viscous damping decreases the displacement demand of the structure (Fig. 4). When the energy dissipation parameter β increases, it reduces the maximum inelastic displacement of SC systems. The effect of energy dissipation parameter is significant for smaller T_1 / T_g ratios than larger T_1 / T_g ratios, especially when $\alpha = 0$.

4.2.3 Influence of post-yield stiffness ratio α

The constant-strength inelastic displacement ratio C_R for $T_1 / T_g \geq 0.75$ does not depend on the increase of post-yield stiffness ratio α (Figs. 2 (e) and (f)). Basically C_R decreases with the increase in α. For example,

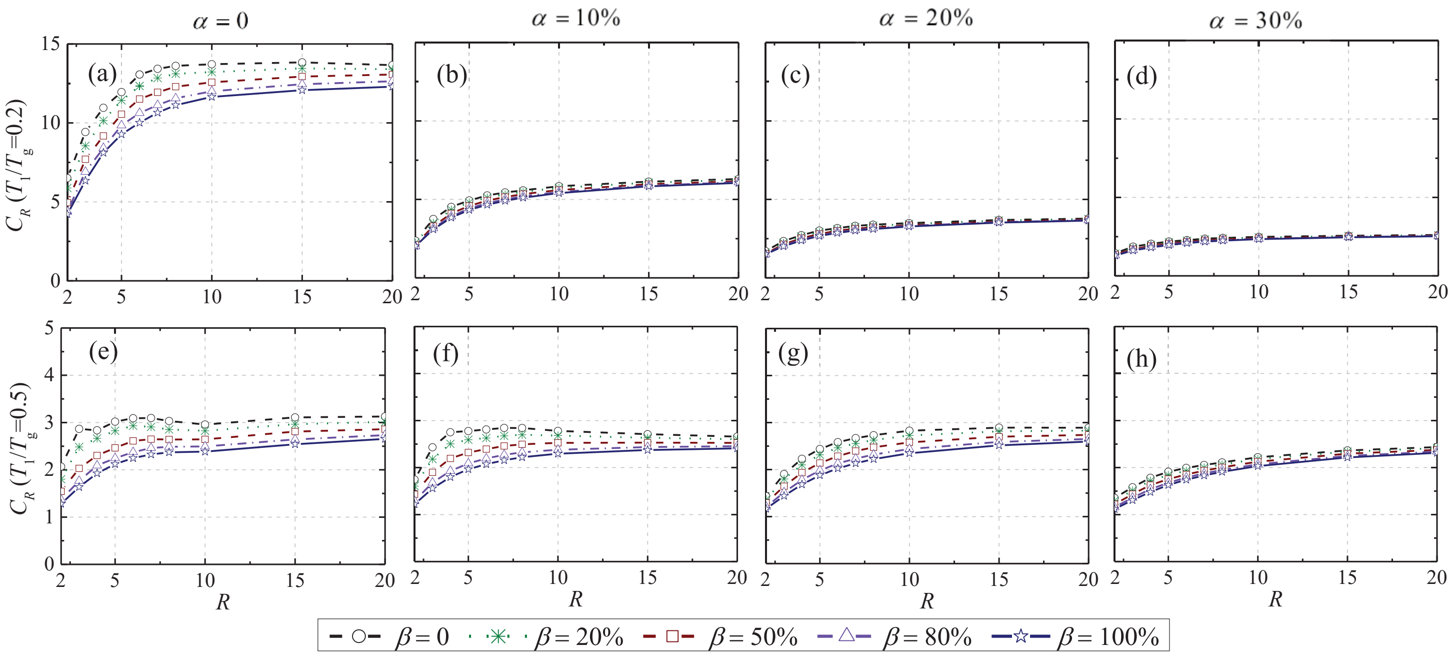

Fig. 3. Mean constant-strength inelastic displacement ratio C_R, variation with response reduction factor R: (a)-(d) $T_1 / T_g = 0.2$; and (e)-(h) $T_1 / T_g = 0.5$.

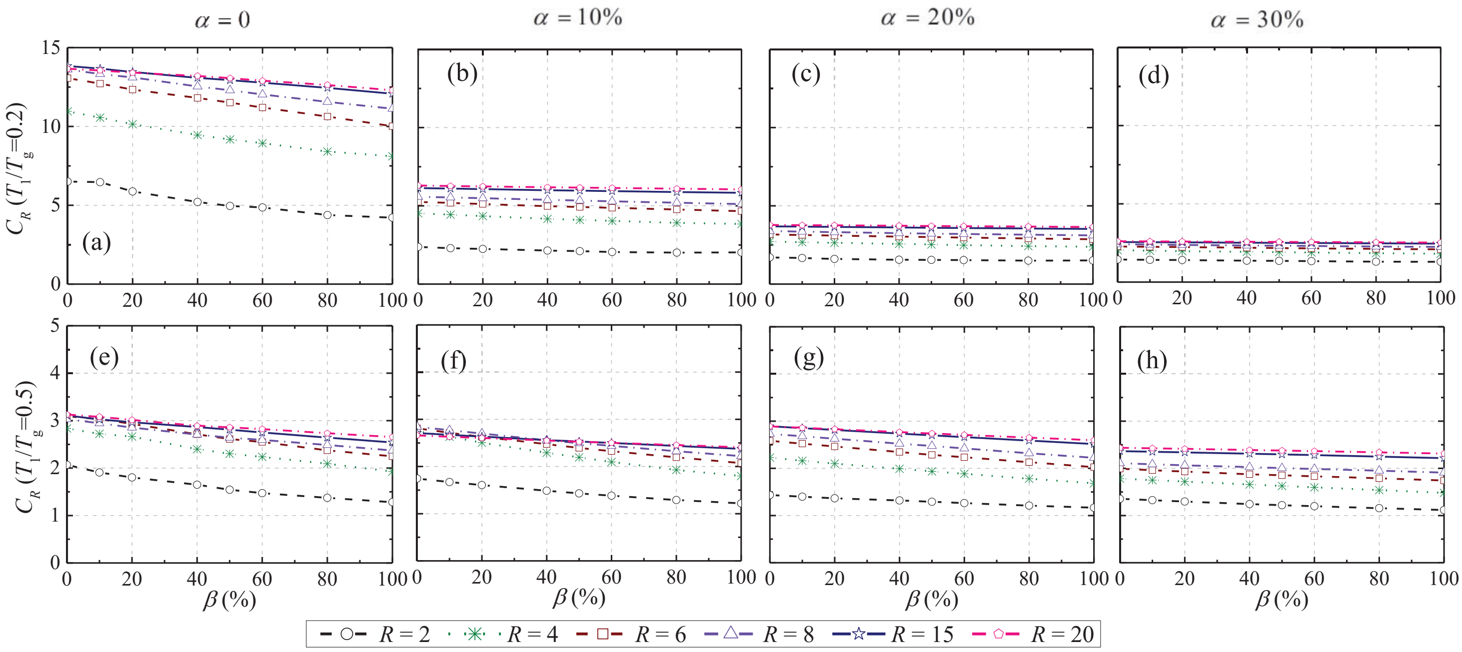

Fig. 4. Mean constant-strength inelastic displacement ratio C_R, variation with hysteretic energy dissipation parameter β: (a)-(d) $T_1 / T_g = 0.2$; and (e)-(h) $T_1 / T_g = 0.5$.

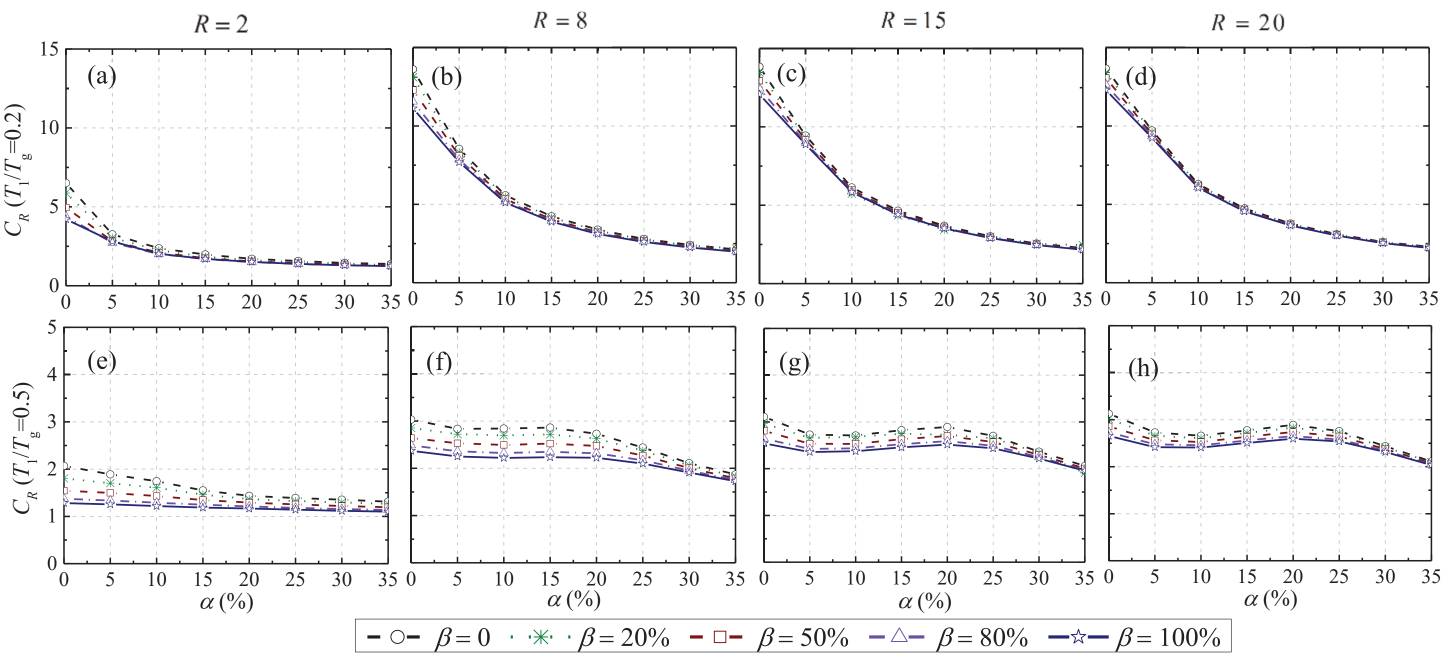

Fig. 5. Mean constant-strength inelastic displacement ratio C_R, variation with post-yield stiffness ratio α: (a)-(d) $T_1 / T_g = 0.2$; and (e)-(h) $T_1 / T_g = 0.5$.

when $T_1 / T_g = 0.2$, $\beta = 80\%$, C_R decreases from 5 to 1.4, 12.3 to 2.0, 12.9 to 2.2 and 13.1 to 2.3 for $R = 2, 8, 15$ and 20, respectively (Figs. 5 (a)-(d)). It can be seen that the effect of the post-yield stiffness ratio α for short periods ($T_1 / T_g < 0.75$) is significant and increase with increasing R. However, for α greater than 35% may not decrease the C_R significantly in all of the cases. On average, 80% decrease of C_R is observed when α increases from 0% to 35% for various SC systems ($R = 2, 8, 15$ and 20) when $T_1 / T_g = 0.2$.

The effect of moderate and large post-yield stiffness ratio can be observed when $T_1/T_g = 0.5$ (Figs. 5 (e)-(h)). It was seen that for moderate post-yield stiffness ratio $0 < \alpha \le 0.15$, the effect is not significant but for large post-yield stiffness ratio $0.15 < \alpha \le 0.35$, the effect is significant.

5. Regression Analysis

As observed from the results in Section 4: (1) the normalized vibration period T_1/T_g results in better characterization of the deformation demands than when using T_1; (2) the influence of the post-yield stiffness ratio α on $C_R - T_1/T_g$ curves is significant for short-periods; and (3) the influence of increasing the hysteretic energy dissipation parameter β to 100%, and the influence of hardening ratio $\alpha \ge 35\%$ is not significant. Hence, improved form of C_R equation is proposed to estimate the constant-strength inelastic displacement ratio of SC systems with flag-shaped hysteretic behavior. The proposed regression equation is,

$$C_R(R,\alpha,\beta,T_1/T_g) = 1 + (R-1)^{b_1}\frac{(b_2 + b_3(1-\beta)^{b_4})(b_5 + b_6(0.35-\alpha)^{b_7})}{(T_1/T_g)^{b_8}} + \\ b_9(T_g/T_1)\exp[b_{10}(\ln(T_1/T_g - 0.02))^2] + b_{11}(T_g/T_1)\exp[b_{12}(\ln(T_1/T_g + 0.5 + 0.02R))^2], \quad (4)$$

where b_1, ..., b_{12} are regression coefficients from the regression analysis.

In the regression analysis, C_R obtained from SDOF systems corresponding to the hysteretic energy dissipation parameter $\beta \le 10\%$ is not included because they tend to dominate the regression. Similarly, the lateral strength ratio $R = 2$ and $R \ge 20$ are not included as they are not practical. The SDOF systems with the post-yield stiffness ratio $\alpha = 0$ are also not included. However, the normalized vibration period T_1/T_g is considered from 0.05 to 3.0. It is important to note here, that the short period region in $C_R - T_1$ curve is not directly equivalent to the lower values of T_1/T_g in $C_R - T_1/T_g$ curve.

The first two terms of the proposed regression equation (Eq. (4)) are similar to Zhang et al. [9]; however, the proposed regression equation includes the functional form of the post-yield stiffness ratio α. Similarly, the last two terms of Eq. (4) are considered similar to the last two terms from Rahgozar et al. [8] realizing the convexity of $C_R - T_1/T_g$ curve. The two-stage fitting (TSF) method is used to determine the regression coefficients. The nonlinear least-squares regression analysis method using the Levenberg-Marquardt Algorithm (LMA) is used for nonlinear regression to determine the fitting coefficients using the statistic package SPSS version 25.0 [13]. At the first stage of the TSF method, the first two terms (C_{R12}) are fitted on the analytical data (C_R^{SDOF}). Then the last two terms are fitted for the difference of the C_R^{SDOF} and C_{R12} to cover the convexity of C_R curve for short T_1/T_g ratios as,

$$C_{R12} = 1 + (R-1)^{b_1}\frac{(b_2 + b_3(1-\beta)^{b_4})(b_5 + b_6(0.35-\alpha)^{b_7})}{(T_1/T_g)^{b_8}}, \quad (5)$$

$$\varepsilon_{C_R} = C_R^{SDOF} - C_{R12}, \\ \approx b_9(T_g/T_1)\exp[b_{10}(\ln(T_1/T_g - 0.02))^2] + b_{11}(T_g/T_1)\exp[b_{12}(\ln(T_1/T_g + 0.5 + 0.02R))^2]. \quad (6)$$

However, the fitted equation could not capture the significant effect of the post-yield stiffness ratio at the short T_1/T_g ratios ($T_1/T_g \le 0.75$). Therefore, an attempt is made to rectify this misfit by using only two initial terms of the proposed regression equation, and the fitting coefficients are recalculated considering moderate post-yield stiffness ratio ($0 < \alpha \le 0.15$) and large post-yield stiffness ratio ($0.15 < \alpha \le 0.35$), for

$T_1/T_g \leq 0.5$ and $T_1/T_g \leq 0.75$, respectively. This is due to the fact that there is no significant effect of post-yield stiffness ratio when $T_1/T_g \geq 0.5$, and $T_1/T_g \geq 0.75$ for C_R ranging $0 < \alpha \leq 0.15$, and $0.15 < \alpha \leq 0.35$, respectively as discussed in Section 4.2.3. Therefore, the fitting coefficients that have been determined for these two groups of SDOF systems with moderate and large post-yield stiffness ratios are shown in Table 2. As shown in Fig. 6, the proposed functional forms could accurately predict C_R on $C_R - T_1/T_g$ plot for all the post-yield stiffness ratios α. It is observed that the proposed regression equation provides better accuracy of C_R at extremely short period and medium-to-long period regions. For the adequacy of the proposed regression equation, the coefficient of determination R^2 as a measure of goodness-of-fit is calculated and $R^2 = 0.953$ and 0.899 are obtained for $0 < \alpha \leq 0.15$, and $0.15 < \alpha \leq 0.35$, respectively.

Table 2. Coefficients from the regression analysis.

	$0 < \alpha \leq 0.15$		$0.15 < \alpha \leq 0.35$	
	$T_1/T_g < 0.5$	$T_1/T_g \geq 0.5$	$T_1/T_g < 0.75$	$T_1/T_g \geq 0.75$
b_1	0.260	0.272	0.277	0.272
b_2	13.038	15.393	1.461	15.393
b_3	1.881	3.247	0.286	3.247
b_4	1.147	1.070	1.337	1.070
b_5	0.045	0.019	0.215	0.019
b_6	17.334	0.200	1.953	0.200
b_7	4.448	24.200	1.306	24.200
b_8	0.397	0.648	0.353	0.648
b_9	-	-0.749	-	-0.749
b_{10}	-	-14.255	-	-14.255
b_{11}	-	0.049	-	0.049
b_{12}	-	-22.396	-	-22.396

Note: The coefficients in column 3 and column 5 are identical.

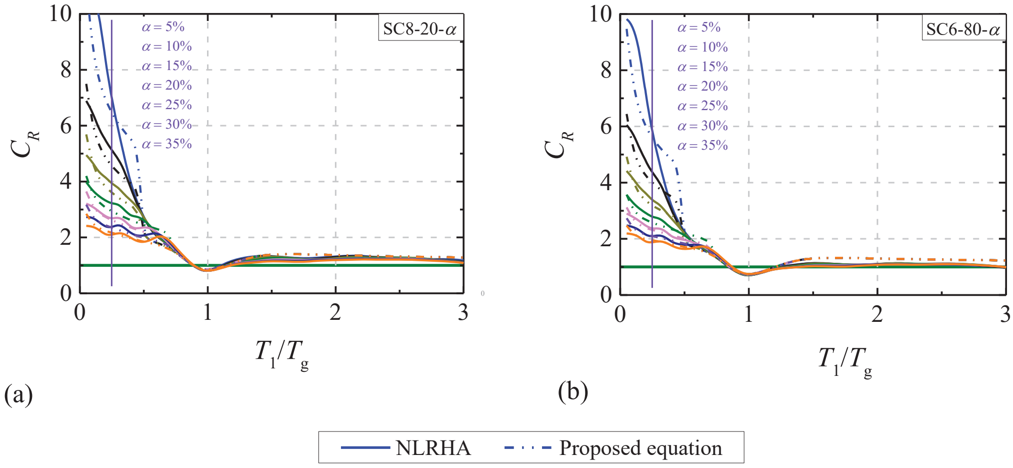

Fig. 6. Comparison of mean constant-strength inelastic displacement ratio C_R, predicted from NLRHA and proposed equation: (a) SC8-20-α system; and (b) SC6-80-α system.

6. Application of C_R on MDOF Systems

The inelastic displacement demand of the flag-shaped hysteretic SDOF system can be well estimated using the proposed regression equation (Eq. (4)), as described in [14] and also in the previous section. It is of great interest whether the proposed regression equation can also estimate the seismic displacement demand of multi-degree-of-freedom (MDOF) systems. For this purpose, several post-tensioned hybrid (PH) precast concrete walls (with flag-shaped hysteretic behavior) are considered. The maximum roof level inelastic seismic demand of PH precast concrete walls is estimated using the inelastic displacement ratio (from Eq. (4)) and the peak roof displacement demand of the linear elastic MDOF system obtained from linear elastic analysis.

6.1 Design of post-tensioned hybrid precast concrete walls

The PH precast concrete walls are designed for 4-, 8-, 10-, and 12-story, five-bay by two-bay reinforced concrete frame buildings (Fig. 7). The floor plan is 35.0 m by 18.0 m with a bay width of 7.0 m in E-W direction and 9.0 m in N-S direction. The floor height is 3.5 m and the slab thickness is 150 mm. The buildings are designed for a location in Los Angeles, California with coordinates 33.949° N, 118.384° W, and the soil is characterized as a stiff soil (site class D). The design spectral response acceleration parameters are $S_{DS} = 1.117g$ and $S_{D1} = 0.615g$ at short periods and 1-s period, respectively. The buildings are intended to be used as school buildings (Risk Category III). Based on the site class, design spectral accelerations, and risk category, the buildings comes under seismic design category D. The two walls in N-S direction are assumed to take all the lateral forces during seismic loading and are considered as the primary lateral load resisting system in N-S direction. The dead load consists of member self-weight, 0.72 kN/m^2 load due to ceiling and mechanical fixtures on slab and 6.8 kN/m load due to partitions and external cladding on floor beams. The floor live load is 4.8 kN/m^2 and roof live load is 1.0 kN/m^2. The seismic weight of the buildings is computed by adding 25% of the live load to the dead load.

The PH precast concrete walls are designed following the guidelines of Smith and Kurama [15] where the design shear forces are distributed along the height of the walls using equivalent lateral force (ELF) procedure. The PH precast concrete walls are designed for two different energy dissipating steel moment ratios $k_d = 0.5$ and 0.8. The 4-story RC frame building PH precast concrete wall with energy dissipating steel moment ratios $k_d = 0.5$ and 0.8 are designated as PH4-50 and PH4-80, respectively. Similar notation is adopted for the other walls.

The design compressive strength of concrete $f'_c = 40$ MPa, the PT tendon initial post-tensioning stress $f_{pi} = 0.55 f_{pu} = 1{,}024$ MPa (with design ultimate stress $f_{pu} = 1{,}862$ MPa), and the yield strength of ED bars is 420 MPa. The PT tendons are anchored at the foundation and roof levels, and unbonded along the height of the wall. The amount of PT tendons and ED steel bars are estimated by satisfying the design moment M_{wd}, using an equivalent rectangular compressive stress distribution at the compression toe of the wall. The design

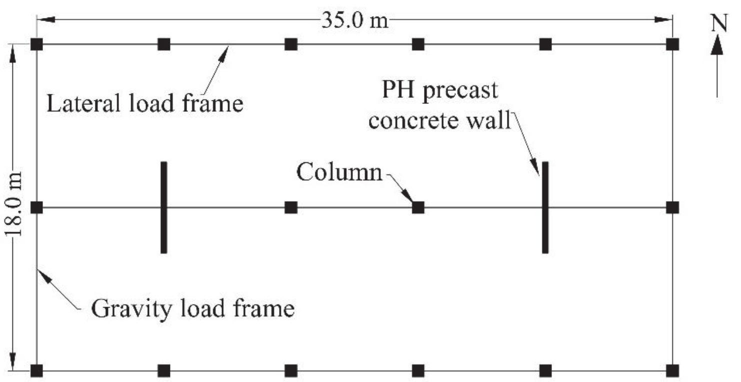

Fig. 7. Plan view of archetype post-tensioned hybrid precast concrete wall buildings.

earthquake (DE) level and risk-targeted maximum considered earthquake (MCE_R) level roof drifts are obtained using the flexural and shear deformation according to ASCE 7 [16]. Under the MCE_R-level roof drift, (1) the PT tendons are designed to remain elastic, (2) the unbonded length of the ED bars are determined to limit the maximum strain in ED steel to less than $0.6\varepsilon_{su}$ (where ε_{su} is the ultimate strain of ED bars = 0.12), and (3) the confinement reinforcement at the base of the PH precast concrete walls is designed to prevent premature crushing of concrete. The design details of all the PH precast concrete walls are shown in Table 3.

6.2 Numerical modeling of post-tensioned hybrid precast concrete walls

The nonlinear fiber element model is used for NLRHA of PH precast concrete walls. The PT tendon is modeled using a *corotational truss* element with *initial strain* material, and the *Steel02* material model provides its hysteretic behavior with a strain hardening ratio of 1%. These tendons are unbonded along the height and are anchored at the top of the wall which is modeled by introducing a *rigid link* constraint between the *corotational truss* element nodes and the *beam-column* element node of the PH precast concrete wall. The ED bars are modeled using *truss* elements with a *Steel02* material model, which are fixed at the foundation level and are kinematically constrained at the top of the milled segment with the corresponding wall node at the height of its unbonded length l_{su}. To simulate the gap opening behavior at the base, the tensile strength of the concrete fibers is set to zero to the height of h_{cr}, defined as critical height by Perez et al. [17]. Above the critical height, the wall panels are modeled with elastic *beam-column* elements. The gross flexural stiffness of the PH precast concrete panels is used in NLRHA. Likewise, the linear elastic models of PH precast concrete walls are also developed. The PH wall elements are modeled using an elastic *beam-column* element and gap opening at base is modeled with effective stiffness recommendation of Smith and Kurama [15]. The post-yield stiffness ratio α is calculated based on recommendations of Wiebe and Christopoulos [18]. The energy dissipation parameter $\beta = 2M_{ws}/(M_{ws}+M_{wp}+M_{wn})$, where M_{ws}, M_{wp} and M_{wn} represent the moment contributions of the ED bars, PT tendons, and wall factored designed gravity load, respectively.

A sub-set of 22 records from the set given in Section 3 were selected and scaled such that the matched spectrum of the earthquake ground motions closely follows the DE-level spectrum in the period range of $0.2T_1 - 1.5T_1$, where the lower bound and upper bound periods are determined from the fundamental periods of 4-story, and 12-story PH precast concrete walls, respectively. Tangent stiffness-based Rayleigh damping with damping ratio $\xi = 3\%$ and 5%, where the damping coefficients are calculated using the first two elastic periods, is used in the NLRHA and linear elastic analysis, respectively.

Table 3. Design details of PH precast concrete walls.

Wall	Response reduction factor (R)	Section size (mm^2)	ρ_p (%)	ρ_s (%)	$P/A_g f'_c$	a_d (mm)	L_{cc} (mm)	l_{su} (mm)
PH4-50	8	400×4000	0.381	0.605	0.037	689.1	790	560
PH4-80	6	400×4500	0.347	0.883	0.033	756.5	860	700
PH8-50	8	400×6500	0.477	0.779	0.051	1214.2	1380	900
PH8-80	6	400×7500	0.396	1.062	0.046	1291.8	1470	1070
PH10-50	8	400×7500	0.608	0.965	0.058	1659.1	1890	930
PH10-80	6	400×8750	0.472	1.249	0.052	1738.8	1980	1100
PH12-50	8	400×8500	0.601	0.984	0.065	1956.8	2230	980
PH12-80	6	400×9750	0.566	1.477	0.060	2150.1	2450	1120

Note: a_d = neutral axis depth; L_{cc} = confinement region length; l_{su} = unbonded length of ED bars; $P/A_g f'_c$ = axial load ratio where P = axial load of wall at the ground level and A_g = cross sectional area of wall; ρ_p = ratio of PT steel area to gross section area of wall; ρ_s = ratio of ED steel area to gross section area of wall.

6.3 Comparison of mean values of inelastic roof displacements predicted using NLRHA with inelastic roof displacements estimated using different equations

The maximum inelastic displacement at roof level of PH precast concrete walls is computed by multiplying C_R with the peak linear elastic displacement at roof level. The mean values of inelastic roof displacements predicted using NLRHA are compared with the inelastic roof displacements estimated in the present study and from Rahgozar et al. [8], and Zhang et al. [9] in Table. 4. The predicted inelastic roof displacements from the present study for both DE and MCE$_R$ levels are closer to the NLRHA results compared to the estimates of Rahgozar et al. [8], and Zhang et al. [9]. Hence the proposed regression equation is capable of estimating inelastic displacement demand for preliminary seismic assessment of PH precast concrete walls. However, for better estimates, MDOF effects such as higher mode effects should be considered.

Table 4. Comparison of the inelastic displacement demands.

Building	T_1 (s)	R	β (%)	α (%)	$\overline{C}_R^{Eq.(4)}$	$\Delta_{Eq.(4)}/\Delta_{NLRHA}$ DE	$\Delta_{Eq.(4)}/\Delta_{NLRHA}$ MCE$_R$	$\Delta_{Rah}/\Delta_{NLRHA}$ DE	$\Delta_{Rah}/\Delta_{NLRHA}$ MCE$_R$	$\Delta_{Zha}/\Delta_{NLRHA}$ DE	$\Delta_{Zha}/\Delta_{NLRHA}$ MCE$_R$
PH4-50	0.612	8	63.1	8.1	1.90	1.38	1.19	4.71	4.06	1.97	1.70
PH4-80	0.514	6	85.2	7.4	1.80	1.24	1.14	3.66	3.88	1.71	1.58
PH8-50	1.189	8	61.6	10.7	1.24	1.30	1.38	2.20	2.33	1.61	1.70
PH8-80	0.693	6	83.7	8.9	1.24	1.01	1.07	1.70	1.79	1.24	1.31
PH10-50	1.542	8	61.3	13.3	1.23	1.44	1.51	1.97	2.07	1.60	1.68
PH10-80	1.230	6	83.3	10.6	1.18	1.23	1.27	1.78	1.83	1.48	1.51
PH12-50	1.847	8	60.7	13.1	1.27	1.40	1.31	1.67	1.56	1.36	1.28
PH12-80	1.512	6	83.2	12.5	1.18	1.31	1.43	1.65	1.80	1.45	1.59

Note: $\overline{C}_R^{Eq.(4)}$ = mean inelastic displacement ratio; $\Delta_{Eq.(4)}$ = inelastic displacement demand using C_R from present study; Δ_{NLRHA} = mean inelastic displacement demand from NLRHA; Δ_{Rah} = mean inelastic displacement demand using Rahgozar et al. [8] (code-compliant form); Δ_{Zha} = mean inelastic displacement demand using Zhang et al. [9].

7. Conclusions

The following conclusions are drawn from this study:

1. The equal displacement rule that has been developed for elasto-plastic hysteretic systems underestimate the inelastic displacement demand of flag-shaped hysteretic structural systems.
2. Normalizing the initial vibration period T_1 with the predominant period of ground motion T_g better characterizes the inelastic displacement demands under far-fault ground motions and show three distinct spectral regions: $T_1/T_g \le 0.85$, $0.85 < T_1/T_g \le 1.2$, and $T_1/T_g > 1.2$.
3. The inelastic displacement demands are highly sensitive to the model parameters; however the effect is not significant when $R > 10$, $\beta \approx 100\%$, and $\alpha > 35\%$.
4. The proposed regression equation is convenient and easy to use compared to previously proposed equations and can estimate the inelastic displacement demand of SC structures to a reasonable degree of accuracy for the extremely short period and medium-to-long period structures.
5. The inelastic roof displacement demand of post-tensioned hybrid precast concrete walls using the present study are much better than the results from available equations.

8. Acknowledgements

The first author gratefully acknowledges a Monbukagakusho (Ministry of Education, Culture, Sports, Science and Technology, Japan) scholarship for graduate students. The authors are pleased to acknowledge financial support from Monbukagakusho under Grant-in Aid for Scientific Research (A) No. 16H02373.

9. References

[1] Veletsos AS, Newmark NM (1960): Effect of inelastic behavior on the response of simple systems to earthquake motions. *Proc. 2nd World Conference on Earthquake Engineering*, Japan, Vol. 2, pp. 895-912.

[2] Veletsos AS, Newmark NM, Chelapati CV (1965): Deformation spectra for elastic and elastoplastic systems subjected to ground shock and earthquake motion. *Proc. 3rd World Conference on Earthquake Engineering*, New Zealand, Vol. II, pp. 663-682.

[3] Ruiz-Garcia J, Miranda E (2006): Inelastic displacement ratios for evaluation of existing structures. *Earthquake Engineering & Structural Dynamics*, **32**, 1237-1258.

[4] Ruiz-Garcia J (2011): Inelastic displacement ratios for seismic assessment of structures subjected to forward-directivity near-fault ground motions. *Journal of Earthquake Engineering*, **15**, 449-468.

[5] Qiang H, Feng P, Qu, Z (2019): Seismic responses of postyield hardening single-degree-of-freedom systems incorporating high-strength elastic material. *Earthquake Engineering & Structural Dynamics*, **48**, 611-633.

[6] Christopoulos C, Filiatrault A, Folz B (2002): Seismic response of self-centring hysteretic SDOF systems. *Earthquake Engineering & Structural Dynamics*, **31**, 1131-1150.

[7] Seo C-Y, Sause R (2005): Ductility demands on self-centering systems under earthquake loading. *ACI Structural Journal*, **102**, 275-285.

[8] Rahgozar N, Moghadam AS, Aziminejad A (2016): Inelastic displacement ratios of fully self-centering controlled rocking systems subjected to near-source pulse-like ground motions. *Engineering Structures*, **108**, 113-133.

[9] Zhang C, Steele TC, Wiebe LDA (2018): Design-level estimation of seismic displacements for self-centering SDOF systems on stiff soil. *Engineering Structures*, **177**, 431-443.

[10] Miranda E (2000): Inelastic displacement ratios for structures on firm sites. *Journal of Structural Engineering* (ASCE), **126** (10), 1150-1159.

[11] OpenSees (2017): *Open System for Earthquake Engineering Simulation*, Computer Program, University of California, Berkeley, California, USA. (Available from: http://opensees.berkeley.edu/ (6 April 2017).

[12] FEMA (2009): *Quantification of building seismic performance factors (FEMA P695)*, Federal Emergency Management Agency (FEMA), Washington, DC, USA.

[13] IBM Corp. (2017): *IBM SPSS Statistics for Windows*, Version 25.0. Armonk, NY: IBM Corp.

[14] Shrestha BK, and Wijeyewickrema AC (2019): Estimation of seismic demands of flag-shaped hysteretic structural systems using inelastic displacement ratios. *5. International Conference on Earthquake Engineering and Seismology (5ICEES),* October 8-11, Middle East Technical University (METU), Ankara, Turkey, Article ID: 10598.

[15] Smith BJ, Kurama Y (2012): Seismic design guidelines for special precast concrete shear walls. *Rep. No. NDSE-2012-02*, University of Notre Dame, Notre Dame, IN.

[16] ASCE (2010): *Minimum Design Loads for Buildings and Other Structures (ASCE 7-10)*, American Society of Civil Engineers (ASCE), Reston, VA, USA.

[17] Perez FJ, Sause R, Pessiki S (2007): Analytical and experimental lateral load behavior of unbonded posttensioned precast concrete walls. *Journal of Structural Engineering* (ASCE), **133** (11), 1531-1540.

[18] Wiebe L, Christopoulos C (2009): Mitigation of higher mode effects in base-rocking systems by using multiple rocking sections. *Journal of Earthquake Engineering*, **13** (S1): 83-108.